Fault Feature Extraction of Rolling Bearing Based on Maximum Second-Order Cyclostationarity Blind Deconvolution and CEEMD-Teager

Hongchang Ding, Xinjie Cheng, Kai Wang and Dewen Pu

College of Mechanical and Electronic Engineering, Shandong University of Science and Technology, Qingdao, People's Republic of China. E-mail: dhchang@sdust.edu.cn

Guangwei Liu

The MOE Key Laboratory of Special Machine and High Voltage Apparatus, Shenyang University of Technology, Shenyang, People's Republic of China.

(Received 18 September 2023; accepted 25 July 2024)

The operation of rolling bearings is directly related to the reliability of the whole rotating machinery. If the rolling bearing failure cannot be diagnosed and repaired in time, it will probably lead to equipment shutdown. The feature extraction process is an important part of bearing fault diagnosis. Some existing feature extraction methods are sensitive to noise and interference, and cannot fully explore and characterize useful information in nonlinear and non-stationary signals in complex scenes, and sometimes even lose important information contained in the data, resulting in low diagnostic accuracy. Therefore, a new method combining Maximum Second-order Cyclostationarity Blind Deconvolution (CYCBD) and Complementary Ensemble Empirical Mode Decomposition (CEEMD) was proposed for feature extraction of rolling bearing faults. Firstly, the cyclic frequency is set according to the failure frequency, and the original signal is filtered by CYCBD. Then, the filtered signal is decomposed into multiple Intrinsic Mode Function (IMF) by CEEMD, and the effective IMF components are selected by kurtosis criterion for reconstruction. Finally, the Teager energy operator is used to enhance the transient impact of the reconstructed signals. The results of simulation and comparison experiments show that the proposed method can extract bearing characteristics in different fault states more effectively, and the accuracy of network model diagnosis is improved compared with the traditional methods.

1. INTRODUCTION

As one of the most common basic components in rotating machinery equipment, rolling bearings are prone to wear, plastic deformation, cracks and other phenomena under the harsh working environment of high speed and heavy load for a long time, so accurate fault diagnosis of bearings is very necessary.[1] The key technology of fault diagnosis lies in fault feature extraction and fault type recognition. In the aspect of feature extraction, vibration analysis is the most practical method to detect rolling bearing faults. When the bearing has been faulty, a series of periodic pulse signals will be generated in the vibration signal, and the fault characteristics can be effectively extracted by analyzing and processing the vibration signals through various algorithms. In terms of pattern recognition, the constantly developing machine learning and deep learning technology has become the mainstream method, and the diagnosis method has gradually developed in the direction of intelligence and automation.[2] Kaplan et al.[3] took the statistical characteristics of vibration signal, such as kurtosis, maximum value and average value, as the input of artificial neural network to realize the bearing defect diagnosis with high accuracy. Li et al.[4] proposed a feature extraction method of discrete random separated spectrum images and combined it with deep learning network for bearing fault diagnosis, finally achieving good accuracy and generalization ability. Kaya et al.[5] successfully diagnosed and predicted bearing fault degree based on time-frequency image features extracted by Continuous Wavelet Transform (CWT). Based on the Wavelet Transform (WT), Bayram et al.[6] obtained the wavelet coefficient which can be used for bearing fault classification. Akcan et al.[7] used different entropy values in vibration signals as the input of the ELM model, and obtained a high classification accuracy.

However, in practical engineering applications, some existing fault diagnosis methods have some limitations in feature extraction effect, anti-interference to noise, and ability of deal with signals in complex environments. To overcome the above limitations, experts and scholars have put forward many improvement and optimization methods. Huang et al.[8] proposed Empirical Mode Decomposition (EMD) in 1988, which has become a milestone of non-stationary signal processing. However, the EMD method has many problems, such as mode mixing, end effect, over-envelope, under-envelope, etc. caused by noise and intermittent signal, which greatly affect its application in practical engineering.[9,10] In 2009, Wu and Huang et al.[11] proposed the ensemble Empirical Mode decomposition (EEMD) method, but the new white noise introduced by this method will cause interference to the original signal and in-

crease the calculation cost.[12]

In 2010, Yes et al.[13] proposed the CEEMD method. By adding two white noise signals with opposite symbols to non-stationary signals and then performing EMD decomposition, the signal decomposition efficiency was successfully improved and the additional interference caused by adding white noise to the original signal by EEMD method was reduced. The residual of additional white noise that persists in IMF is eliminated, the IMF reconstruction error is reduced, and the calculation time is saved. In view of IMF component reconstruction after CEEMD decomposition, Sahu et al.[14] carried out Adaptive Threshold Denoising (ATD) for noise-dominated IMF components obtained after CEEMD decomposition and tested the effectiveness of the proposed denoised signals on the experimental data set. Ke et al.[15] used the global optimality of Genetic Algorithm (GA) to optimize the white noise amplitude in EEMD, and then processed the optimized Gaussian white noise signal through CEEMD, and finally successfully applied it in bearing fault diagnosis. Gong et al.[16] decomposed and reconstructed the Horizontal Visibility Graph (HVG) by CEEMD method, and reflected the local geometric features of vibration signals through the horizontal visibility relationship. Gu et al.[17] combined CEEMD with Permutation Entropy (PE) to achieve a good decomposition of rolling bearing vibration signals by taking advantage of the randomness detection of PE signals.

The Blind Deconvolution (BD) theory has obvious effect in the process of bearing fault pulse extraction.[18] The inverse filtering coefficient is obtained by solving the maximum or minimum criteria of different convolution objects, and then the fault period or quasi-periodic pulse is extracted from the original signal.[19,20] One of the most commonly used BD algorithms is the Minimum Entropy Deconvolution (MED) proposed by WIGGINS,[21] which uses kurtosis as the objective function. However, kurtosis is very sensitive to large random pulses and cannot distinguish periodic pulse from random pulse, so it is only suitable for extracting a single periodic pulse.[22] In 2012, McDonald et al.[23] proposed Maximum Correlated Kurtosis Deconvolution (MCKD) method, which highlighted periodic pulse components on the basis of correlated kurtosis. However, MCKD has poor adaptive ability, and the selection of parameters such as filter length and convolution period has a great influence on the results.[24]

Buzzoni et al.[25] proposed the method called CYCBD in 2018. Based on maximizing the second-order cyclostationarity (ICS_2), the periodic part of the impact energy in the original signal was considered by introducing cycle frequency parameter. Ke et al.[26] used CYCBD for early fault feature extraction of common rail injectors, and input extracted fault features into Least Squares Support Vector Machine (LSSVM) to successfully complete fault identification and classification. Wang et al.[27] improved CYCBD. The cyclic frequency is estimated by the autocorrelation function of morphological envelope. The performance efficiency ratio index combined with the equal-step search strategy was proposed to determine the filter length. The experimental results on the gearbox fault test platform show that the improved CYCBD can accurately extract the bearing fault frequency. Zhang et al.[28] used Envelope Harmonic Product Spectrum (EHPS) to accurately estimate cycle frequency, which greatly improved the practical application value of CYCBD.

In summary, the existing fault feature extraction methods have some defects, such as sensitivity to noise, limited extraction ability in complex environment and information loss. The approach presented in this paper aims to overcome these limitations by combining CEEMD with CYCBD. CEEMD method has strong anti-noise ability and focuses on capturing different frequency characteristics of global signals, while CYCBD method focuses on analyzing local characteristics such as periodic characteristics and correlation in signals. The two methods complement each other's information and can well adapt to the extraction task in complex environments. At the same time, with the assistance of Teager energy operator, the noise is further suppressed, which provides convenience for the subsequent network model diagnosis.

The content of this paper was arranged as follows: the basic theory, the overall process of feature extraction method, simulation analysis, comparative experimental verification, and conclusion.

2. THEORY BACKGROUND

2.1. CYCBD

Blind Deconvolution is a technique that can extract pulse components from observed signals. Its core purpose is to construct an inverse filter to extract noiseless fault signals from noisy original signals. The mathematical expression is as follows:

$$s = x * h = (s_0 * g) * h \approx s_0. \tag{1}$$

Where s is the calculated source signal, s_0 is the target source signal, x is the mixed signal, g is the unknown impulse response function, h is the inverse filter to be sought, and $*$ represents the convolution operation. It can be expressed in matrix form as follows:

$$\boldsymbol{s} = \boldsymbol{X}\boldsymbol{h}; \tag{2}$$

$$\begin{bmatrix} s_{N-1} \\ \vdots \\ s_{L-1} \end{bmatrix} = \begin{bmatrix} x_{N-1} & \cdots & x_0 \\ \vdots & \ddots & \vdots \\ x_{L-1} & \cdots & x_{L-N-1} \end{bmatrix} \times \begin{bmatrix} h_0 \\ \vdots \\ h_{N-1} \end{bmatrix}. \tag{3}$$

Where L and N represent the length of signal sampling and the length of inverse filter, respectively.

The cyclostationarity process can be used to describe the vibration signals of rotating machinery with periodic statistical characteristics, in which some periodic information of the second-order cyclostationarity (ICS_2), characterizing the periodic fluctuation of the signal energy, indicates the occurrence of faults. CYCBD is a blind deconvolution method based on generalized Rayleigh Entropy, which aims to maximize ICS_2 and achieve the purpose of fault feature extraction. Formula (4)– (8) give the general definition of ICS_2 matrix.

$$ICS_2 = \frac{\boldsymbol{h}^H \boldsymbol{X}^H \boldsymbol{W} \boldsymbol{X} \boldsymbol{h}}{\boldsymbol{h}^H \boldsymbol{X}^H \boldsymbol{X} \boldsymbol{h}} = \frac{\boldsymbol{h}^H \boldsymbol{R}_{XWX} \boldsymbol{h}}{\boldsymbol{h}^H \boldsymbol{R}_{XX} \boldsymbol{h}}; \tag{4}$$

$$\boldsymbol{W} = diag(\frac{P\left[|\boldsymbol{s}|^2\right]}{\boldsymbol{s}^H\boldsymbol{s}})(L-N+1) = \begin{bmatrix} \ddots & & 0 \\ & P\left[|\boldsymbol{s}|^2\right] & \\ 0 & & \ddots \end{bmatrix} \frac{(L-N+1)}{\sum_{l=N-1}^{L-1}|\boldsymbol{s}|^2}; \quad (5)$$

$$P\left[|\boldsymbol{s}|^2\right] = \frac{1}{L-N+1}\sum \boldsymbol{e}_k(\boldsymbol{e}_k^H|\boldsymbol{s}|^2) = \frac{\boldsymbol{E}\boldsymbol{E}^H|\boldsymbol{s}|^2}{L-N+1}; \quad (6)$$

$$\boldsymbol{E} = \left[\boldsymbol{e}_1 \quad \cdots \quad \boldsymbol{e}_k\right]; \quad (7)$$

$$e_k = \left(e^{-j2\pi\frac{k}{T_S}l} \quad \cdots \quad e^{-j2\pi\frac{k}{T_S}(L-1)}\right)^T. \quad (8)$$

In the above formula, $\boldsymbol{R}_{XWX}$ and $\boldsymbol{R}_{XX}$ are weighted correlation matrix and correlation matrix respectively, $\boldsymbol{W}$ is the weighted matrix, k is the number of samples, T_s indicates the fault period.

According to the properties of generalized Rayleigh entropy, the optimal filter $\boldsymbol{h}$ is obtained by solving the maximum eigenvalue λ, then the maximum ICS_2 is obtained:

$$\boldsymbol{R}_{XWX}\boldsymbol{h} = \boldsymbol{R}_{XX}\boldsymbol{h}\lambda. \quad (9)$$

The specific steps of initializing the filter h and setting the iterative error ε to iteratively solve the optimal filter are shown in Fig. 1.

2.2. CEEMD

Complementary Ensemble Empirical Mode Decomposition is a derivative method of EMD. By adding positive and negative pairs of Gaussian white noise into the original signal and then using EMD decomposition to calculate the average value, this method not only effectively suppressed the mode aliasing effect, but also overcame the disadvantages of low computational efficiency of EEMD and large influence of white noise residue, significantly improved the signal-to-noise ratio after IMF component reconstruction and reduced the reconstruction error. The details of the CEEMD method are as follows:

1. The M groups of Gaussian white noise with the same amplitude and opposite sign are added to the original signal.

$$\begin{bmatrix} y_i^+(t) \\ y_i^-(t) \end{bmatrix} = \begin{bmatrix} 1 & 1 \\ 1 & -1 \end{bmatrix} \begin{bmatrix} x(t) \\ n_i(t) \end{bmatrix}. \quad (10)$$

   Where $i = 1, 2, ..., M$, $x(t)$ as the original signal, and $n_i(t)$ is the additional ith Gaussian white noise signal.

2. A series of IMF sets $c_{ij}^+(t)$, $c_{ij}^-(t)$ and residuals are obtained by EMD decomposition of $2M$ mixed signals $y_i^+(t)$ and $y_i^-(t)$ respectively. Where $c_{ij}(t)$ represents the jth IMF component obtained after adding the ith noise. Detailed introduction of EMD is described by Huang.[8]

3. By summing and averaging IMF components corresponding to the above M groups, the final IMF components of each order are calculated as follows:

$$IMF_j = \frac{1}{2M}\sum_{i=1}^{M}\left[c_{ij}^+(t) + c_{ij}^-(t)\right]. \quad (11)$$

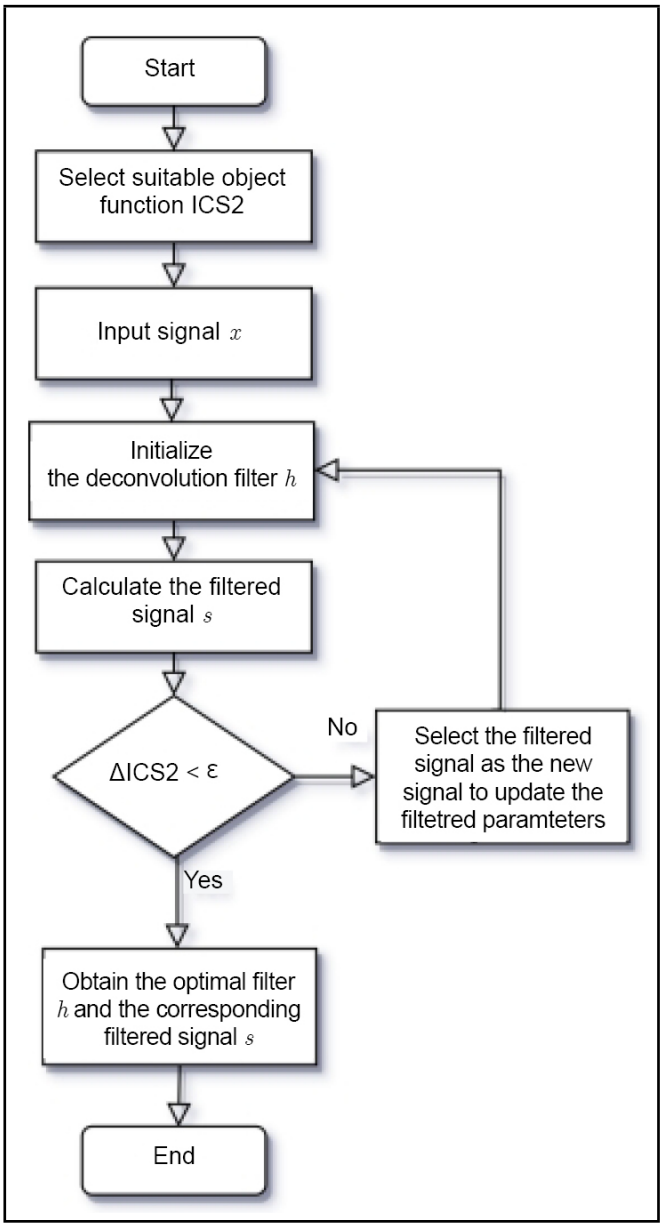

Figure 1. Iterative solution of the optimal filter.

Finally, the original signal $x(t)$ can be decomposed into a series of IMF components and a residual $r_n(t)$:

$$x(t) = \sum_{j=1}^{N} IMF_j + r_n(t). \quad (12)$$

2.3. Teager Energy Operator

Teager energy operator is a nonlinear operator used to calculate signal energy. For continuous signal $s(t)$, Teager energy operator is defined as:

$$\varphi\left[s(t)\right] = \left[\dot{s}(t)\right]^2 - s(t)\ddot{s}(t). \quad (13)$$

Where $\dot{s}(t)$ and $\ddot{s}(t)$ represent the first and second differential of the measured signal $s(t)$ at time t, respectively.

For discrete signal $s(n)$, difference is used to instead of differential, and only three discrete points are used in each calculation, so it has good time resolution and demodulation speed. The Teager energy operator of discrete point can be expressed

as:

$$\varphi\left[s(n)\right] = \left[s(n)\right]^2 - s(n+1)s(n-1). \tag{14}$$

Different from the traditional definition of signal energy as the square of signal amplitude, the Teager energy operator is more sensitive to transient components, and the output is the square of instantaneous amplitude multiplied by the square of instantaneous frequency. Therefore, Teager energy operator can effectively detect the sudden change of energy flow and enhance the characteristics of high-frequency transient shock.

3. THE PROPOSED FAULT FEATURE EXTRACTION METHOD OF ROLLING BEARING

Based on the advantages of CYCBD and CEEMD methods, a rolling bearing fault feature extraction method was proposed in this paper. The specific process is shown in Fig. 2. The main steps of this method were as follows:

1. Step 1: Acceleration sensor was used to collect vibration signal of rolling bearing.
2. Step 2: Selecting the appropriate filter length, the bearing failure frequency was obtained by the theoretical formula to set the cycle frequency set, the maximum number of iterations and convergence criteria.
3. Step 3: CYCBD was used to filter signals for noise reduction.
4. Step 4: Performing CEEMD decomposition on the filtered signal to obtain a series of IMF components arranged from high frequency to low frequency.
5. Step 5: Calculating the kurtosis value of each IMF component. According to the kurtosis criterion, the kurtosis will increase significantly when bearing faults occur, so the IMF components with kurtosis value greater than 3 were selected for signal reconstruction.
6. Step 6: Using Teager energy operator to improve the impact characteristics of the reconstructed signal.
7. Step 7: Analyzing the envelope spectrum of the signal processed by Teager energy operator and extracting clear fault features.

4. SIMULATED ANALYSIS

To verify the effectiveness of the proposed fault feature extraction method, the bearing outer ring fault was simulated by using periodic unilateral attenuation pulse signal $x(t)$ and harmonic component $s(t)$ mixed with Gaussian white noise $n(t)$. The constructed simulation $y(t)$ can be expressed as:

$$\begin{cases} y(t) = x(t) + s(t) + n(t) \\ x(t) = y_0 e^{-\zeta\omega_n t}\sin\left(\omega_n t\sqrt{1-\zeta^2}\right) \\ \omega_n = 2\pi f_n \\ s(t) = A_0\sin\left(2\pi f_0 t\right) + A_1\sin\left(2\pi f_1 t\right) + \\ \qquad A_2\sin\left(2\pi f_2 t\right) \end{cases}. \tag{15}$$

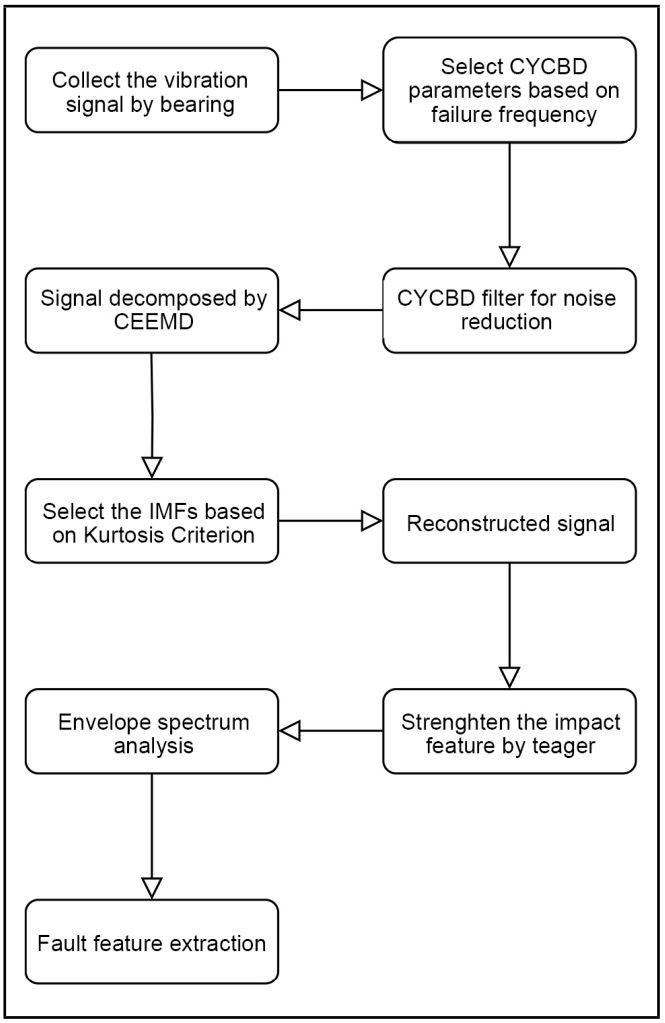

Figure 2. Specific process of fault feature extraction.

Where y_0 was 0.3 for displacement coefficient, f_n was 3000 Hz for natural frequency of bearing, and ζ was 0.035 for damping coefficient. A_0, A_1 and A_2 were 0.15, 0.1 and 0.2 respectively, representing the amplitude of interference harmonics, f_0, f_1 and f_2 were 5, 75 and 150 respectively, representing the frequency of interference harmonics. $n(t)$ is Gaussian white noise. After adding noise, the SNR of $y(t)$ was -10 dB. Under the condition of sampling frequency 12000 Hz, 8192 data points are collected, and the pulse period is set to 0.01 s, so the fault frequency is 100 Hz. The time domain diagram of the fault simulation signal of the bearing outer ring is shown in Fig. 3.

The Hilbert envelope spectrum below 1500 Hz of the simulation signal is shown in Fig. 4. Due to noise and harmonic interference, the periodic pulse component with a frequency of 100Hz in the signal has been completely covered without any fault related information. To extract the periodic pulse component clearly, according to the fault feature extraction method proposed in this paper, the hybrid simulation signal was firstly filtered by CYCBD to reduce the noise interference. The filter length was 400 and the cyclic frequency set of 100 Hz and its multiples was constructed according to the pulse signal frequency. The filtered envelope spectrum of the simulated signal is shown in Fig. 5. Compared with the stage before filtering, part of the noise interference component in the signal is fil-

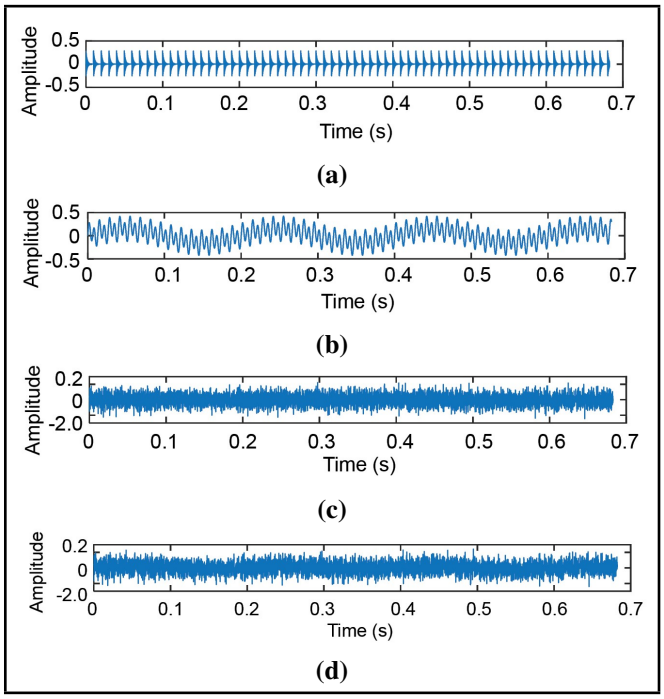

Figure 3. Simulation signals: (a) periodic unilateral attenuation pulse signal; (b) Harmonic components; (c) Gaussian white noise; (d) Mixed signals.

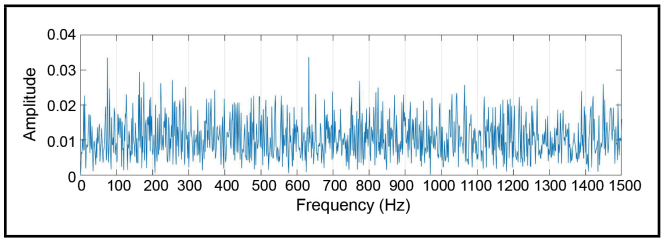

Figure 4. Envelope spectrum of original simulated signal.

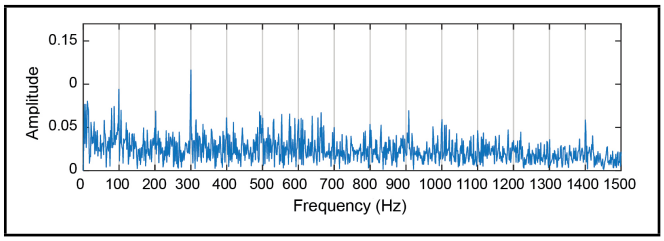

Figure 5. Envelope spectrum of simulated signal after CYCBD filtering.

tered out, the periodic pulse component begins to appear, and the amplitude of the triple frequency component is the most obvious. Then, the filtered simulation signal was decomposed by CEEMD, and the signal was decomposed into 11 IMF components from high frequency to low frequency and a residual, as shown in Fig. 6 and Fig. 7. Then, relevant IMF components were selected for reconstruction according to the kurtosis criterion. The kurtosis values of each IMF component are shown in Table 1. Then, the instantaneous energy of the signal is calculated by using the Teager energy operator to highlight the periodic pulse part of the signal. The time domain waveform of the reconstructed signal and instantaneous Teager energy are shown in Fig. 8. Finally, through the envelope analysis of

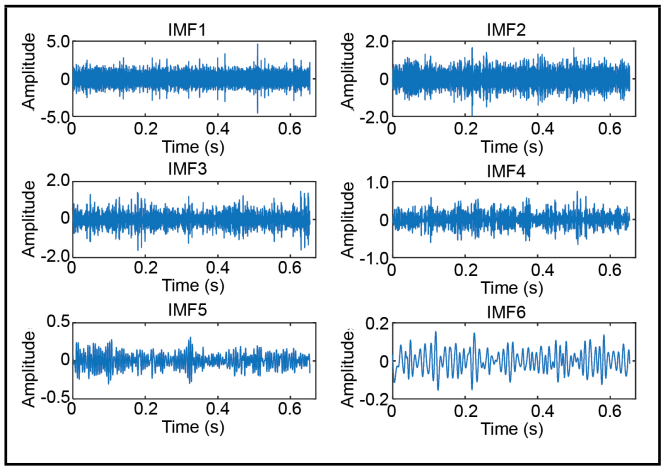

Figure 6. High-frequency components of IMF.

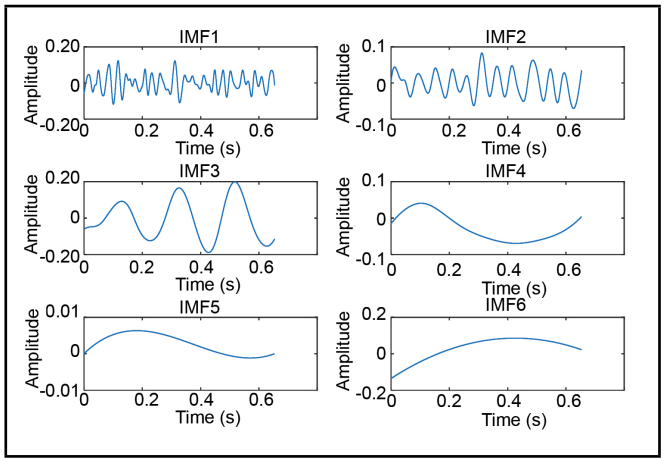

Figure 7. Low-frequency component and residual of IMF.

Table 1. The kurtosis of the IMF components.

IMF	IMF1	IMF2	IMF3	IMF4	IMF5	IMF6
kurtosis	3.160	3.302	4.097	3.264	2.864	2.764
IMF	IMF7	IMF8	IMF9	IMF10	IMF11	
kurtosis	2.631	3.3663	2.031	1.904	1.455	

the instantaneous energy waveform of Teager, clear and accurate fault characteristic frequency and frequency doubling are obtained, as shown in Fig. 9. Simulation results show that the proposed method can effectively extract the impact feature information under multiple interference states.

5. EXPERIMENTAL VALIDATION

5.1. Case 1: Rotating Machinery Transmission Parts Fault Implantation Test Bench

To explore the fault feature extraction effect of the proposed method, a comparative study of several fault feature frequency extraction methods was carried out using the bearing vibration data collected by the rotating machinery transmission component fault implantation test rig. The test platform is shown in Fig. 10, equipped with a three-phase asynchronous motor and connected the load plate, bearing seat, planetary gear box and powder brake through the coupling. The acceleration sensor

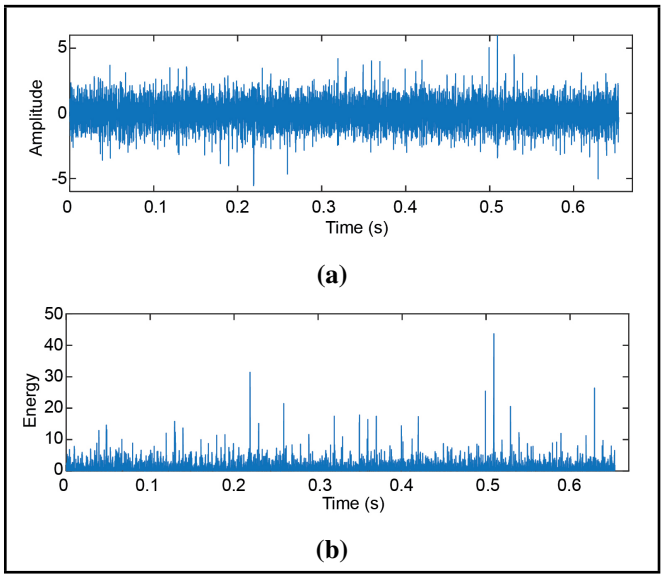

Figure 8. (a) Time domain waveform of reconstructed signal; (b) Instantaneous Teager energy.

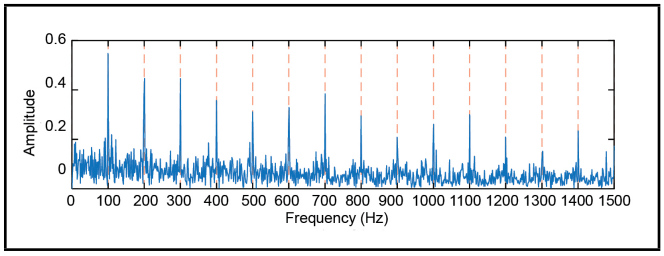

Figure 9. Envelope spectrum of Teager energy waveform.

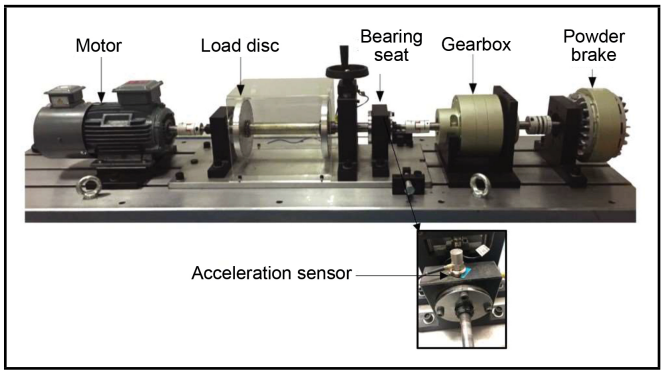

Figure 10. Bearing fault signal collection experiment platform.

is vertically placed above the bearing, and the bearing vibration signal is collected by data acquisition board. The bearing model used in the test is 6205, and the relevant parameters are shown in Table 2.

Under the condition of sampling frequency 12000 Hz and motor speed 1000 RPM, the vibration signals of healthy bearing and outer ring fault, inner ring fault and ball fault of 0.2 mm and 0.4 mm were collected respectively. The test bearings in various states are shown in Fig. 11. According to formula (16)–(18), the fault characteristic frequencies of inner ring, outer ring and ball are 90.17 Hz, 59.83 Hz and 78.50 Hz, respectively.

$$f_{IF} = 0.5z\left(1 + \frac{d}{D}\cos\alpha\right)\frac{n}{60}; \tag{16}$$

Table 2. Geometric parameters of the bearing.

Bearing type	6205-2RS JEM SKF
Inside Diameter	0.9843 in
Outside Diameter	2.0472 in
Thickness	0.5906 in
Number of rollers	9
Ball Diameter	0.3126 in
Pitch Diameter	1.537 in
Contact Angle	0°

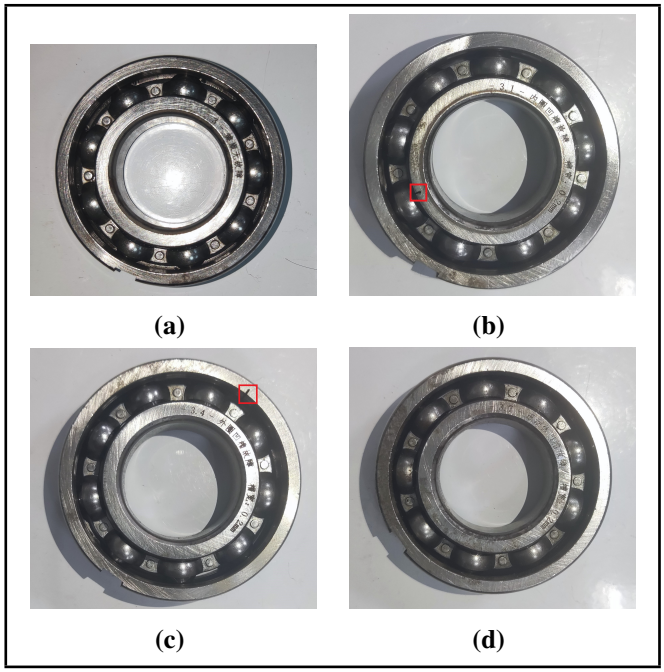

Figure 11. Fault condition of bearing type 6205.

$$f_{OF} = 0.5z\left(1 - \frac{d}{D}\cos\alpha\right)\frac{n}{60}; \tag{17}$$

$$f_{BF} = \frac{D}{d}\left(1 - \left(\frac{d}{D}\right)^2\cos^2\alpha\right)\frac{n}{60}. \tag{18}$$

Where f_{IF}, f_{OF}, and f_{BF} were the inner ring failure frequency, outer ring failure frequency and rolling element failure frequency, z was the number of rolling element, d was the diameter of rolling element, D was the raceway pitch diameter, α was the bearing contact Angle, and n was the speed.

Each state was collected for 5 seconds, and 12000 data points were randomly selected for repeated analysis. The signal with outer ring fault size width of 0.4 mm was taken as an example. It shows the time domain waveform and the original envelope spectrum of the fault signal with the fault size of 0.4 mm outer ring in Fig. 12. In the envelope spectrum, rotation frequency dominates, and no other fault frequency was reflected.

The final envelope spectrum of the original signal processed by the method proposed in this paper is shown in Fig. 13(a). Bearing fault feature extraction methods of Maximum Correlation Kurtosis Deconvolution and Complementary Ensemble Empirical Mode Decomposition (MCKD-CEEMD),[29] Minimum Entropy Deconvolution and Local Mean Decomposition (MED-LMD),[30] Variational Mode Decomposition and Maximum Correlation Kurtosis Deconvolution (MCKD-VMD),[31]

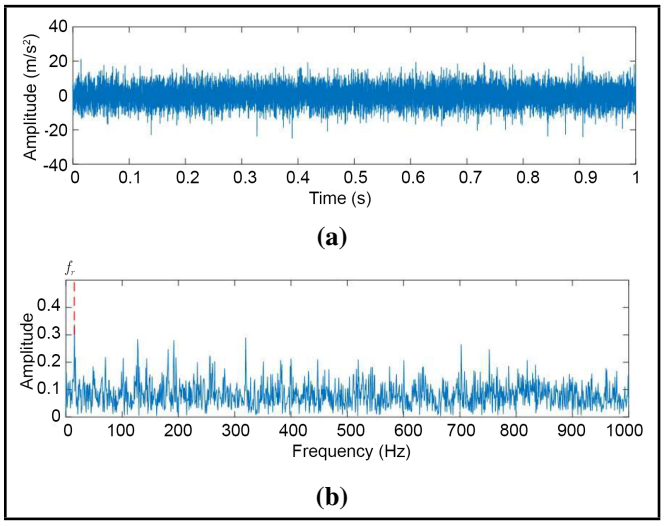

Figure 12. Failure signal of 0.4 mm outer ring: (a) time domain diagram; (b) envelope spectrum.

proposed by previous scholars, were used to extract vibration signals analyze. To ensure the minimum experimental variables, the filter length of various methods was the same as that of CYCBD method, and the number of iterations was 50. It shows the final envelope spectrum obtained after MCKD-CEEMD treatment in Fig. 13(b). Firstly, MCKD was used to filter the fault signal. After CEEMD decomposition, IMF component with a mutual relation number greater than 0.5 with the original signal was selected for reconstruction. LMD was a very effective fault signal processing method with high decomposition efficiency and good effect on non-stationary signal processing. Using MED method to preprocess the signal can improve the decomposition accuracy of LMD, reduce the number of decomposition layers and improve the signal-to-noise ratio. The final envelope spectrum obtained after MED-LMD processing of fault signal is shown in Fig. 13(c). The final envelope spectrum obtained after MCKD-VMD processing of fault signals is shown in Fig. 13(d), where the penalty factor of VMD was 3000 and the number of decomposed modes was 5. After the reconstructed signal is obtained, MCKD is used to enhance the weak fault characteristics of the bearing.

As the envelope spectrum shown in Fig. 13(a), the fault characteristic frequency and high-order harmonics of the bearing outer ring are clearly visible, and the amplitude of the fundamental frequency is more than 1.5, and the noise interference is greatly suppressed, which effectively improves the sensitivity of fault identification. In Fig. 13(b), the failure frequency and rotation frequency of the bearing outer ring dominate. The second and third harmonics of the rotation frequency and the harmonics of the failure frequency of the bearing outer ring can also be detected in the envelope spectrum. In Fig. 13(c), the rotation frequency and outer ring failure frequency and their harmonics can be clearly detected. In Fig. 13(d), the characteristic frequency of the outer ring fault and its first four orders of harmonics all exist in prominent peaks. By introducing evaluation index P,[32] the processing performance of different methods are compared with each other. The comparison results of the four methods are shown in Table 3. Where, the evaluation index P is defined as the ratio of the energy of the fault

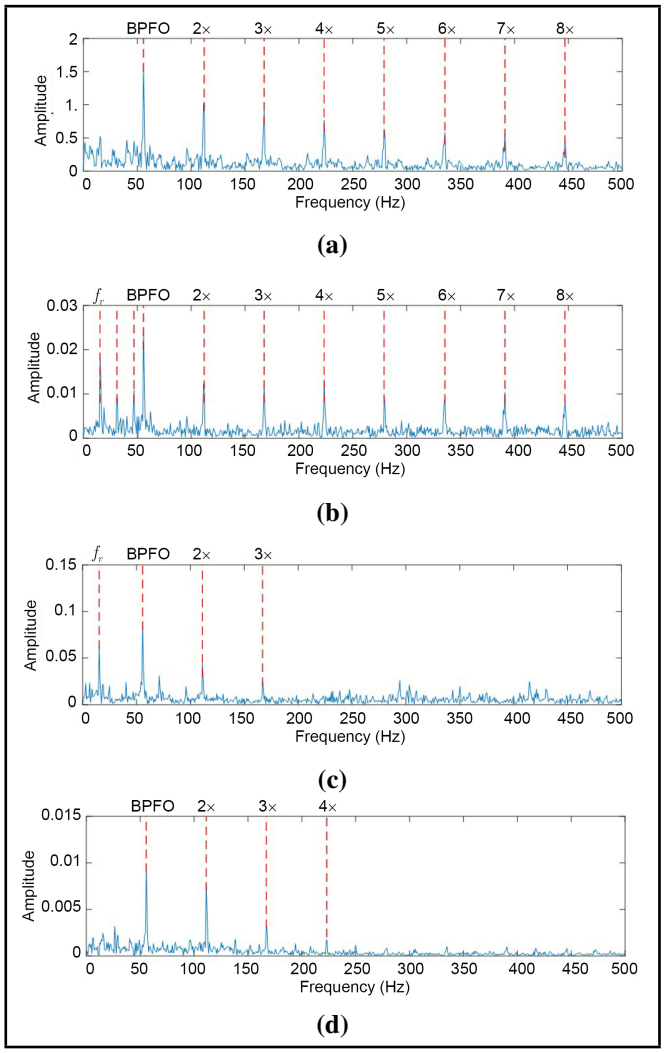

Figure 13. Envelope spectra of different treatment methods: (a) CYCBD-CEEMD-Teager; (b) MCKD-CEEMD; (c) MED-LMD; (d) MCKD-VMD.

characteristic component to the total energy in the envelope spectrum, which can be calculated according to the following formula:

$$p = \frac{\sum [A(f)]^2}{\sum [A(f)]^2 + \sum [A(f')]^2} \times 100\%. \tag{19}$$

Where f and f' are fault component and noise component respectively, $A(f)$ and $A(f')$ are their amplitudes in the envelope spectrum respectively.

It can be seen from Table 3 that all the four methods can detect the fault characteristic frequency, but the method proposed in this paper can detect the highest amplitude of fault frequency and the most relevant harmonic components. The value of evaluation index P is also the largest, indicating that the energy proportion of fault characteristic component is the highest, and the influence of interference component on fault characteristics is the least. Therefore, the method proposed in this paper can extract more obvious fault features and has better results in fault diagnosis.

5.2. Case 2: CWRU Bearing Data Set

To further evaluate the effectiveness of the feature extraction method proposed in this paper, the open bearing data from

Table 3. Comparative results of different methods.

methods	The comparison of fault extraction results									P
	f_i	$2f_i$	$3f_i$	$4f_i$	$5f_i$	$6f_i$	$7f_i$	$8f_i$	Failure frequency amplitude	
CYCBD-CEEMD-Teager	✓	✓	✓	✓	✓	✓	✓	✓	1.502	27.71%
MCKD-CEEMD	✓	✓	✓	✓	✓	✓	✓	✓	0.024	20.98%
MED-LMD	✓	✓	✓	×	×	×	×	×	0.092	19.39%
MCKD-VMD	✓	✓	✓	✓	×	×	×	×	0.011	23.84%

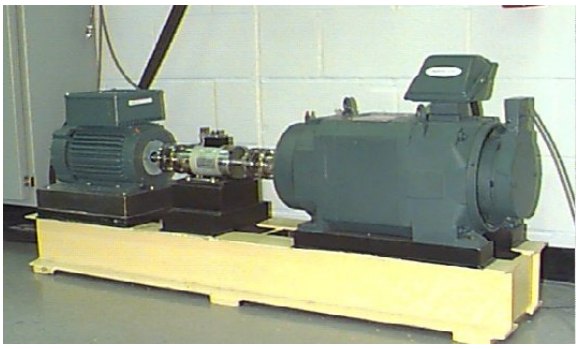

Figure 14. The CWRU bearing test platform.

Case Western Reserve University (CWRU) was used to conduct an experimental study of fault classification. The experimental platform for data acquisition is shown in Fig. 14, which was driven by a 1.5Kw three-phase induction motor and connected to a dynamometer by torque sensor and decoder and coupling. The driving end bearing model is deep groove ball bearing 6205-2RS JEM SKF. Single point faults of different sizes were introduced in different parts through electric discharge machining, and bearing vibration signals were collected by acceleration sensors. According to a reference study on CWRU bearing data proposed by Smith et al.,[33] three signals of different fault types, highly disturbed by noise and difficult to extract fault feature (N1), are selected for experimental analysis in this paper. The details of the selected fault signals are shown in Table 4.

When the sampling frequency was 12 kHz, 100 samples were randomly selected for each fault signal, each sample contained 4096 data points, and all samples were processed according to the proposed feature extraction method. The length of CYCBD filter is 300. In the process of CEEMD decomposition, 8 times of ensemble average processing were carried out, and the ratio of the standard deviation of the amplitude of white noise to the standard deviation of the amplitude of the original signal was selected as 0.2. The final envelope analysis results are shown in Fig. 15.

Due to the motor speed error, the inevitable bearing manufacturing size deviation and long-term wear and other reasons, there was a slight deviation between the above fault characteristic frequency and the theoretical calculation, but it was within the acceptable range. Based on model transfer theory of transfer learning, this paper introduces ResNet-18 network model to realize fault classification. ResNet-18 is a deep learning neural network model designed by Microsoft Research Asia on the basis of traditional convolutional neural networks, and is one of the residual neural network series. The model belongs to a lightweight model, which is suitable for use under the condition of limited resources. To adapt the input size of the network model, all samples after feature extraction were saved as $224 \times 224 \times 3$ RGB three-channel JPEG format images, and 40 samples under each fault were used for training and the remaining samples were used for testing. The setting of hyperparameters in the network model is adjusted by many tests. The selection of model hyperparameters is shown in Table 5.

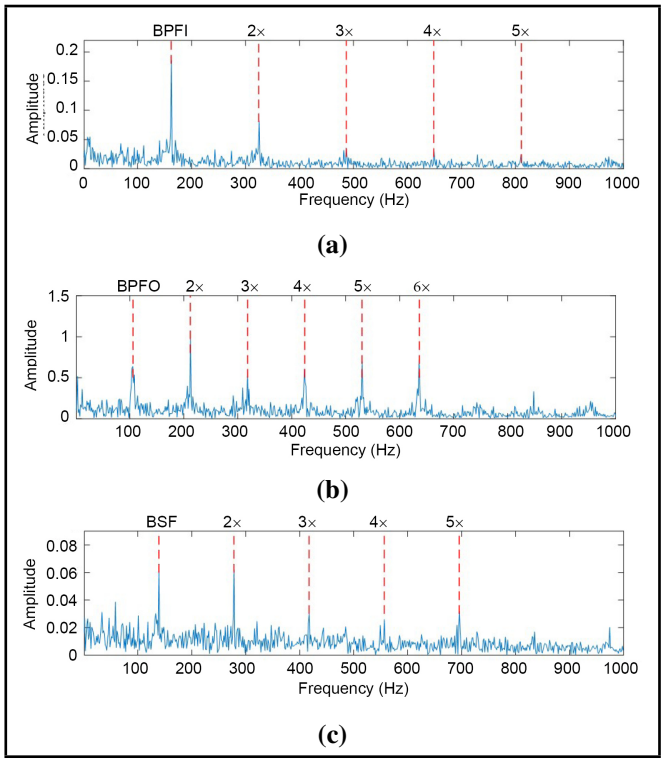

Figure 15. Envelope spectrum of different fault signals: (a) inner race; (b) outer race; (c) ball.

Fig. 16 shows the final accuracy curve and cross entropy loss curve of the smoothed test set. The results show that the convergence speed of the classification network model is fast, and the accuracy of the model is high after 10 iterations, and the final accuracy reaches 100%. The loss curve also rapidly converges to about 0.03, which indicates that the model has a good fitting ability for the task.

Table 6 compares the diagnostic performance of the proposed method with the results of other studies. It can be seen from the table that in multiple studies using Case Western Reserve University data as the benchmark, the accuracy of fault diagnosis using the method proposed in this paper is higher than most other methods.

6. CONCLUSION

In this paper, a bearing fault feature extraction method based on CYCBD and CEEMD is proposed. Firstly, by selecting relevant parameters, the original signal is filtered by CYCBD and

Table 4. Details about the fault signal.

File number	Fault type	Motor speed (rpm)	Load (hp)	Fault diameter (in)	Fault depth (in)	Failure frequency (Hz)
3001	inner race fault (IF)	1797	0	0.028	0.05	162.18
200	outer race fault (OF)	1772	1	0.014	0.011	106.02
119	ball fault (BF)	1772	1	0.007	0.011	139.10

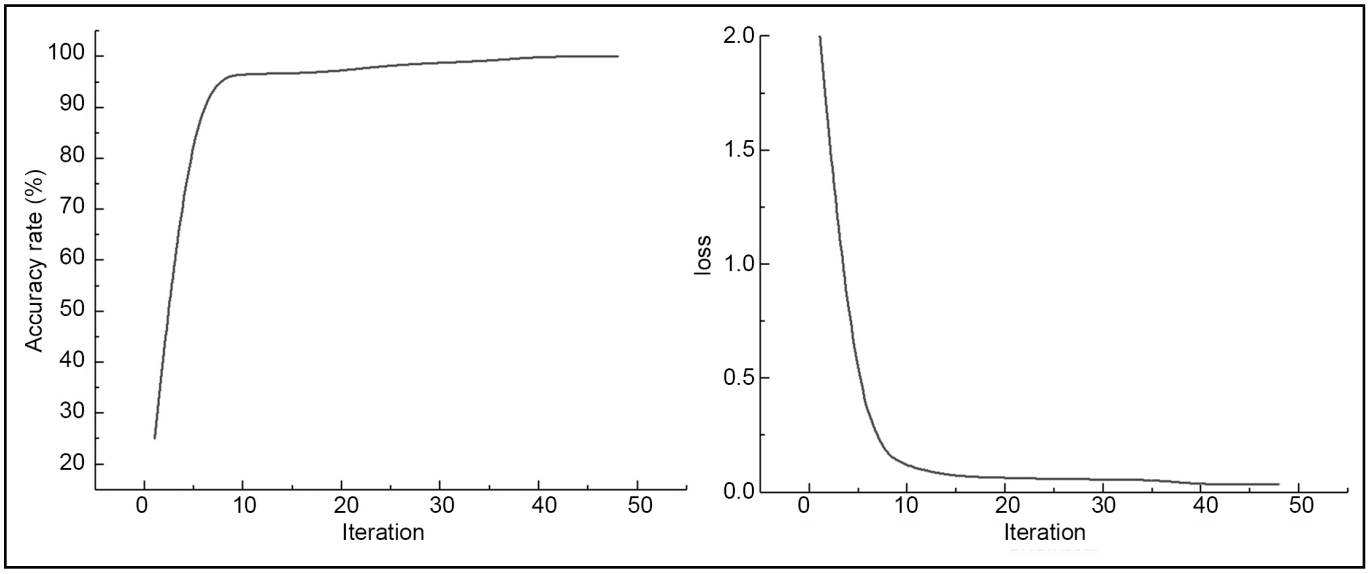

Figure 16. Network model final accuracy and loss curve.

Table 5. Network model hyperparameter Settings.

Number	Hyperparameter	Set value
1	optimizer	SGD
2	Initial learning rate	0.001
3	Batch size	64
4	Iteration rounds	8
5	Verification frequency	5
6	Gradient clipping mode/Threshold	L2/1
7	Momentum term attenuation coefficient	0.9

decomposed by CEEMD. Then, the IMF components are selected by kurtosis criterion for signal reconstruction. Finally, the Teager energy operator is used to process the signal to realize the feature extraction of the complex signal. The results of simulation and comparison experiments show that the proposed method can clearly extract the fault features contained in the signal. The residual network model is introduced to identify the faults of CWRU bearing data after feature extraction, and the final accuracy rate reaches 100%. Compared with the existing methods, this method has the following advantages. On the one hand, nonlinear components and time-varying information in the whole signal can be captured by CEEMD, local periodic information in the signal can be extracted by CYCBD. The combination of the two algorithms can realize information complementarity, which effectively avoid data information loss and realize deep discovery of fault characteristic information. On the other hand, the Teager energy operator method is introduced in this paper to enhance the weak impact signal hidden in the noise, strengthen the difference between different fault characteristics, and effectively improve the comprehensiveness and accuracy of diagnosis. In addition, the method involves human intervention to find the optimal parameters, as well as the problems of occupying computing resources and consuming time costs. In the future, research will focus on improving the adaptability and real-time performance of fault feature extraction to improve the reliability and efficiency of diagnosis.

ACKNOWLEDGEMENT

This research has been supported by Key Laboratory of Special Machine and High Voltage Apparatus (Shenyang University of Technology), Ministry of Education (KFKT202202). The supports are gratefully acknowledged.

CONFLICT OF INTEREST

The authors declare no conflict of interest, financial or otherwise.

REFERENCES

[1] Liu, Z. and Zhang, L. A review of failure modes, condition monitoring and fault diagnosis methods for large-scale wind turbinenbearings, *Measurement,* **149**, (2020). https://doi.org/10.1016/j.measurement.2019.107002

[2] Zhao, H., Yang, X., Chen, B., Chen, H., and Deng, W. Bearing fault diagnosis using transfer learning and optimized deep belief network, *Measurement Science and Technology*, **33** (6), (2022). https://doi.org/10.1088/1361-6501/ac543a

[3] Kaplan, K., Bayram, S., Kuncan, M., and Ertun, H. M. Feature Extraction of Ball Bearings in Time-Space and Estimation of Fault Size with Method of ANN, *Proceedings of the 16th Mechatronika 2014*, (2014).

Table 6. Comparison of results with those from the literature.

Author(s)	Method	Dataset	Fault Type	Accuracy
Kuncan[34]	1D-LBP+GRA	Author's setup	NS, ORF, IRF, BF	99%–100%
Kaplan et al.[35]	Signal2Image+LBP	Author's setup	NS, ORF, IRF, BF	100%
Kaya et al.[36]	1D-GLCM+RF	Author's setup	NS, ORF, IRF, BF	99.3%
Li et al.[37]	DSLS-SVM	CWRU setup	NS, ORF, IRF, BF	99.90%
Liu et al.[38]	GRU-NP-DAEs	CWRU setup	NS, ORF, IRF, BF	99.75%
Ahmed et al.[39]	CS-LS-LRC	CWRU setup	NS, ORF, IRF, BF	99.9%
Zhu et al.[40]	MFME	CWRU setup	NS, ORF, IRF, BF	90.95%–100%
Chen et al.[41]	RS-DFV	CWRU setup	NS, ORF, IRF, BF	99.47%–100%
Authors of this article	CYCBD-CEEMD-Teager+ResNet 18	CWRU setup	NS, ORF, IRF, BF	100%

[4] Li, Z., Wang, H., Chen, J., Zhou, Z., and Chen, W. Research on Rolling Bearing Fault Diagnosis Based on DRS Frequency Spectrum Image and Deep Learning, *International Journal of Acoustics and Vibration*, **28** (2), 211–219, (2023). https://doi.org/10.20855/ijav.2023.28.21942

[5] Kaya, Y. Kuncan, F., and Ertunç, H. M. A new automatic bearing fault size diagnosis using time-frequency images of CWT and deep transfer learning methods, *Turkish Journal of Electrical Engineering and Computer Sciences*, **30** (5), 1851–1867, (2022). https://doi.org/10.55730/1300-0632.3909

[6] Bayram, S., Kaplan, K., Kuncan, M., and Ertunc, H. The effect of bearings faults to coefficients obtaned by using wavelet transform, *22nd Signal ProcessingCommunications Applications Conference*, 991–994, (2014). https://doi.org/10.1109/SIU.2014.6830398

[7] Akcan, E., Kuncan, M., Kaplan, K., and Kaya, Y. Diagnosing bearing fault location, size, and rotational speed with entropy variables using extreme learning machine, *Journal of the Brazilian Society of Mechanical Sciences and Engineering*, **46** (1), 4, (2024). doi10.1007/s40430-023-04567-2

[8] Huang, N. E. *et al*. The Empirical Mode Decomposition and the Hilbert Spectrum for Nonlinear and Non-Stationary Time Series Analysis, *Proceedings: Mathematical, Physical and Engineering Sciences*, **454** (1971), (1998).

[9] Randall, R. B. and Antoni, J. Why EMD and similar decompositions are of little benefit for bearing diagnostics, *Mechanical Systems and Signal Processing*, **192**, (2023). https://doi.org/10.1016/j.ymssp.2023.110207

[10] Rato, R. T., Ortigueira, M. D., and Batista, A. G. On the HHT, its problems, and some solutions, *Mechanical Systems and Signal Processing*, **22** (6), (2007). https://doi.org/%5b3%5d10.1016/j.ymssp.2007.11.028.

[11] Wu, Z. and Huang, N. E. Ensemble Empirical Mode Decomposition: a Noise-Assisted Data Analysis Method, *Adv. Data Sci. Adapt. Anal.*, **1**, 1–41, (2009). https://doi.org/10.1142/S1793536909000047

[12] Damine, Y., Bessous, N., Pusca, R., Megherbi, A. C., Romary, R., and Sbaa, S. A New Bearing Fault Detection Strategy Based on Combined Modes Ensemble Empirical Mode Decomposition, KMAD, and an Enhanced Deconvolution Process, *Energies*, **16** (6), (2023). https://doi.org/10.3390/en16062604

[13] Yeh, J. R., Shieh, J. S., and Huang, N. E. Complementary Ensemble Empirical Mode Decomposition: a Novel Noise Enhanced Data Analysis Method, *Adv. Data Sci. Adapt. Anal.*, **2**, 135–156, (2010). https://doi.org/10.1142/S1793536910000422

[14] Kumar, S. P. and Nandan, R. R. Fault Diagnosis of Rolling Bearing Based on an Improved Denoising Technique Using Complete Ensemble Empirical Mode Decomposition and Adaptive Thresholding Method, *Journal of Vibration Engineering & Technologies*, **11** (2), (2022). https://doi.org/%5b2%5d10.1007/S42417-022-00591-Z.

[15] Ke, Z., Di, C., and Bao, X. Adaptive Suppression of Mode Mixing in CEEMD Based on Genetic Algorithm for Motor Bearing Fault Diagnosis, *IEEE Transactions on Magnetics*, **58** (2), 1–6, (2022). https://doi.org/10.1109/tmag.2021.3082138

[16] Gong, X., Feng, K., Zhi, Z., Gao, Y., and Du, W. Multiple fault diagnosis for rolling bearings method employing CEEMD-GCN based on horizontal visibility graph, *Measurement Science and Technology*, **34** (3), (2023). https://doi.org/10.1088/1361-6501/aca706

[17] Gu, J. and Peng, Y. An improved complementary ensemble empirical mode decomposition method and its application in rolling bearing fault diagnosis, *Digital Signal Processing*, **113**, (2021). https://doi.org/10.1016/j.dsp.2021.103050

[18] Wang, J., Zhang, F., Zhang, L., and Jiang, M. Maximum average impulse energy ratio deconvolution and its application for periodic fault impulses enhancement of rolling bearing, *Advanced Engineering Informatics*, **53**, (2022). https://doi.org/10.1016/j.aei.2022.101721

[19] Liang, K., Zhao, M., Lin, J., Jiao, J., and Ding, C. Maximum average kurtosis deconvolution and its application for the impulsive fault feature enhancement of rotating machinery, *Mechanical Systems and Signal Processing*, **149**, (2021). https://doi.org/10.1016/j.ymssp.2020.107323

[20] Had, A. and Sabri, K. A two-stage blind deconvolution strategy for bearing fault vibration signals, *Mechanical Systems and Signal Processing*, **134**, (2019). https://doi.org/10.1016/j.ymssp.2019.106307

[21] Endo, H. and Randall, R. B. Enhancement of autoregressive model based gear tooth fault detection technique by the use of minimum entropy deconvolution filter, *Mechanical Systems and Signal Processing*, **21** (2), (2006). https://doi.org/10.1016/j.ymssp.2006.02.005.

[22] Xu, Y., Cai, Z., Cai, X., and Ding, K. An enhanced multipoint optimal minimum entropy deconvolution approach for bearing fault detection of spur gearbox, *Journal of Mechanical Science and Technology*, **33** (6), 2573–2586, (2019). https://doi.org/10.1007/s12206-019-0505-9

[23] McDonald, G. L., Zhao, Q., and Zuo, M. J. Maximum correlated Kurtosis deconvolution and application on gear tooth chip fault detection, *Mechanical Systems and Signal Processing*, **33**, 237–255, (2012). https://doi.org/10.1016/j.ymssp.2012.06.010

[24] Tian, T., Tang, G. J., Tian,Y. C., and Wang, X. L. Blind Deconvolution Based on Correlation Spectral Negentropy for Bearing Fault, *Entropy (Basel)*, **25** (3), (2023). https://doi.org/10.3390/e25030543

[25] Buzzoni, M., Antoni, J., and D'Elia, G. Blind deconvolution based on cyclostationarity maximization and its application to fault identification, *Journal of Sound and Vibration*, **432**, 569–601, (2018). https://doi.org/10.1016/j.jsv.2018.06.055

[26] Ke, Y., Yao, C., Song, E., Dong, Q., and Yang, L. An early fault diagnosis method of common-rail injector based on improved CYCBD and hierarchical fluctuation dispersion entropy, *Digital Signal Processing*, **114**, (2021). https://doi.org/10.1016/j.dsp.2021.103049

[27] Wang, Z., Zhou, J., Du, W., Lei, Y., and Wang, J. Bearing fault diagnosis method based on adaptive maximum cyclostationarity blind deconvolution, *Mechanical Systems and Signal Processing*, **162**, (2022). https://doi.org/10.1016/j.ymssp.2021.108018

[28] Zhang, B., Miao, Y., Lin, J., and Yi, Y. Adaptive maximum second-order cyclostationarity blind deconvolution and its application for locomotive bearing fault diagnosis, *Mechanical Systems and Signal Processing*, **158**, (2021). https://doi.org/10.1016/j.ymssp.2021.107736

[29] Wang, F., Liu, C., Su, W., Xue, Z., Han, Q., and Li, H. Combined Failure Diagnosis of Slewing Bearings Based on MCKD-CEEMD-ApEn, *Shock and Vibration*, **2018**, 1–13, (2018). https://doi.org/10.1155/2018/6321785

[30] Wang, Z., Wang, J., Kou, Y., Zhang, J., Ning, S., and Zhao, Z. Weak Fault Diagnosis of Wind Turbine Gearboxes Based on MED-LMD, *Entropy*, **19** (6), (2017).

[31] Cui, H., Guan, Y., and Chen, H. Rolling Element Fault Diagnosis Based on VMD and Sensitivity MCKD, *IEEE Access*, **9**, 120297–120308, (2021). https://doi.org/10.1109/access.2021.3108972

[32] Zhao, H. and Li, L. Fault diagnosis of wind turbine bearing based on variational mode decomposition and Teager energy operator, *IET Renewable Power Generation*, **11** (4), (2017). https://doi.org/10.1049/iet-rpg.2016.0070

[33] Smith, W. A. and Randall, R. B. Rolling element bearing diagnostics using the Case Western Reserve University data: A benchmark study, *Mechanical Systems and Signal Processing*, **64–65**, 100–131, (2015). https://doi.org/10.1016/j.ymssp.2015.04.021

[34] Kuncan, M. An Intelligent Approach for Bearing Fault Diagnosis: Combination of 1D-LBP and GRA, *Ieee Access*, **8**, 137517–137529, (2020). https://doi.org/10.1109/access.2020.3011980

[35] Kaplan, K., Kaya, Y., Kuncan, M., Minaz, M. R., and Ertunc, H. M. An improved feature extraction method using texture analysis with LBP for bearing fault diagnosis, *Applied Soft Computing*, **87**, 106019, (2020). https://doi.org/10.1016/j.asoc.2019.106019

[36] Kaya, Y., Kuncan, M., Kaplan, K., Minaz, M. R., and Ertunc, H. M. A new feature extraction approach based on one dimensional gray level co-occurrence matrices for bearing fault classification, *Journal of Experimental & Theoretical Artificial Intelligence*, **33** (1), 161–178, (2021). https://doi.org/10.1080/0952813x.2020.1735530

[37] Li, X., Yang, Y., Pan, H., Cheng, J., and Cheng, J. A novel deep stacking least squares support vector machine for rolling bearing fault diagnosis, *Computers in Industry*, **110**, 36–47, (2019). https://doi.org/10.1016/j.compind.2019.05.005

[38] Liu, H., Zhou, J., Zheng, Y., Jiang, W., and Zhang, Y. Fault diagnosis of rolling bearings with recurrent neural network based autoencoders, *Isa Transactions*, **77**, 167–178, (2018). https://doi.org/10.1016/j.isatra.2018.04.005

[39] Ahmed, H. and Nandi, A. K. Compressive Sampling and Feature Ranking Framework for Bearing Fault Classification With Vibration Signals, *Ieee Access*, **6**, 44731–44746, (2018). https://doi.org/10.1109/access.2018.2865116

[40] Zhu, K., Chen, L., and Hu, X. A Multi-scale Fuzzy Measure Entropy and Infinite Feature Selection Based Approach for Rolling Bearing Fault Diagnosis, *Journal of Nondestructive Evaluation*, **38** (4), 90, (2019). https://doi.org/10.1007/s10921-019-0623-4

[41] Chen, X., Zhang, X., Zhou, J., and Zhou, K. Rolling Bearings Fault Diagnosis Based on Tree Heuristic Feature Selection and the Dependent Feature Vector Combined with Rough Sets, *Applied Sciences-Basel*, **9** (6), 1161, (2019). https://doi.org/10.3390/app9061161